Qualitative evaluation of a parabolic mirror with substructured Ronchi gratings

M. Campos-García

Instituto de Ciencias Aplicadas y Tecnología, Universidad Nacional Autónoma de México,
Circuito Exterior S/N, Ciudad Universitaria, 04510, Ciudad de México.

F. Granados-Agustín

Instituto Nacional de Astrofísica óptica y Electrónica,
Apartado Postal 51 and 216, 72000 Puebla, Pue, México

D. Aguirre-Aguirre

Instituto de Ciencias Aplicadas y Tecnología, Universidad Nacional Autónoma de México, Circuito Exterior S/N, Ciudad
Universitaria, 04510, Ciudad de México.

V. Iván Moreno-Oliva

Universidad del Istmo, Ciudad Universitaria S/N, C.P. 70760, Tehuantepec, Oax. México.

O. Huerta-Carranza

Instituto Nacional de Astrofísica óptica y Electrónica Apartado Postal 51 and 216, 72000 Puebla, Pue, México.

In this work, we propose to qualitatively test a concave parabolic mirror by means of the Ronchi interferometric test using substructured gratings to increase the sharpness of the fringes. The substructured gratings are designed considering that the grating period is divided into several stripes of equal width that can be transparent or opaque; the transmission coefficients of the stripes along the grating period are not periodic, but a previously chosen binary sequence. Equations were derived to obtain the corresponding intensity profiles and an analysis of these profiles was performed for different sequences and positions of the substructured gratings with respect to the test mirror. It was experimentally verified that the fringes are sharper at the Rayleigh distance inside and outside the mirror focus.

Keywords: Ronchi interferometric; Rayleigh distance.

1. Introduction

The Ronchi test is an optical test widely used in the optical workshop to test concave mirrors [1]. Normally, the test is performed qualitatively, providing a subjective evaluation of the surface under test. However, quantitative information on local surface manufacturing errors can also be obtained. During the manufacturing process of an optical surface, it is necessary to verify its quality. As a result, several analytic techniques and methods have been developed. Among them, the Ronchi test stands out as one of the preferred techniques in the optics workshop, as it is one of the simplest and widely used methods to qualitatively measure the wavefront of an optical system when observed at the pupil exit; this test has been the subject of numerous publications and extensive reviews [2]. Recently, a new approach has been developed to describe Ronchi's non-paraxial geometric test for evaluating spherical mirrors using an inverse ray tracing procedure [3]. This procedure allows the evaluation of geometrical parameters such as radius of curvature, source coordinates, and positions and orientation of the detection and grating planes from the Ronchigrams.

The simple Ronchi test setup consists of using a grating, which is a set of equally spaced transparent and opaque slits, and a point or extended light source. The grating is placed near the center of curvature of the test surface, as schematized in Fig. 1.The source is located off-axis, so that fringe images are formed at the exit pupil of the optical system. The shape of the fringes observed at the pupil of the optical system, and recorded by a camera, depends on the aberrations of the optical system and can be explained using the interpretation of geometrical optics, where the black fringes are shadows of the black stripes of the grating; it can also be explained from the point of view of physical optics, interpreting the fringes as produced by the lateral shear interference of the light diffracted by the gratings, considered as a diffractive grating [4, 5]. Recently, a phase-shifted Ronchi test procedure has been developed to obtain the figure of a parabolic mirror using a bi-Ronchi grating [6]. Similarly, another procedure uses two mutually perpendicular classical Ronchi gratings to perform the test accurately [7, 8].

The main advantage of the geometric Ronchi test is its simplicity since it requires only the grating and the light source; it does not require a special optical system. Its main disadvantage is that the intensity profiles cannot be calculated in the geometrical optics regime. However, it is possible to perform an interference-based analysis to obtain fringe intensity profiles [1,3,9]. On the other hand, to increase the sharpness of the fringes observed in the interference patterns in Ronchi test, a configuration of unequal widths of the opaque

and transparent slits of the grating is used [10]. In this case, the widths of the stripes (transparent or opaque) are unequal; they can be considered positive if the width of the transparent stripes is greater than that of the opaque stripes, and negative if the width of the opaque stripes is greater than that of the transparent stripes. On the other hand, the use of liquid crystal display (LCD) for Ronchi grid display has been widely used due to its versatility in strip display; however, the LCD must be properly calibrated as discussed in some references where LCD is used for Ronchi grid display [6,11-14]. In Ref. [11] a variable frequency grating and LCD were used to test optical surfaces. Here a combination of several Ronchi gratings was used to create the substructure of the variable frequency grating. Examples of such substructured gratings are generalized Moirè gratings called Katyl gratings [15]. Here, each grating period is divided into several stripes of equal width that can be transparent or opaque; the transmission coefficients for the stripes along the grating period are not periodic, but a previously chosen binary sequence.

According to previous works [16,17], to perform the test of a concave parabolic mirror we must evaluate the position where the Talbot images appear. This position is related to the Rayleigh distance and gives us the position where we should place the grating to obtain an image that is a perfect replica of the object's grating. We performed a numerical analysis for a parabolic mirror, and obtained the intensity profiles for the proposed substructured grating and found that the sharpness of the fringes is high when the defocus of the Ronchi grating is equal to Rayleigh distance, and half of the Rayleigh distance. Furthermore, we found that for positions Ronchi grating equal to one-quarter and three-quarters of the Rayleigh distance the fringe contrast is completely lost.

In this paper, we propose the use two 8-bit substructured gratings, one positive and one negative, to increase the sharpness of the fringes. Additionally, we develop a theoretical framework to obtain the intensity profile of the Ronchi test using these substructured gratings. For this purpose, in Sec. 2, we develop analytical expressions to obtain the corresponding intensity profiles. Then, in Sec. 3 we propose substructured a Katyl-type gratings to perform an analysis of these profiles and of the sharpness of the fringes for some sequences and positions of the gratings. Section 4 describes the procedure for calculating the distances at which the Ronchi grating should be placed to increase the fringe sharpness considering a parabolic wavefront at the exit pupil of the optical system. In Sec. 5 we present experimental results related to the testing of a parabolic mirror. Finally, in Sec. 6 we present our conclusions.

2. Interference pattern in the Ronchi test

To calculate the intensity pattern in the interferometric Ronchi test in the detection plane we must consider the schematic diagram of a Ronchi test for a converging wavefront, as shown in Fig. 1. Thus, in the far-field regime, the
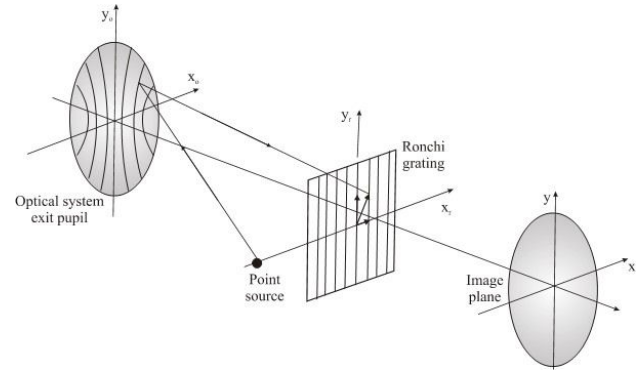

FIGURE 1. Typical arrangement for the Ronchi test considering convergent wavefronts.

diffracted field $a(x_r, y_r)$ in the plane of the grating is given by

$$a(x_r, y_r) = \int\int\limits_{-\infty}^{\infty} A(x_o, y_o) e^{\frac{-i2\pi(x_r x_o + y_r x_o)}{\lambda r}} dx_o dy_o, \quad (1)$$

where r is the radius of curvature of the reference spherical wavefront, and the function $A(x_o, y_o)$ is the pupil function, given by

$$A(x_o, y_o) = \begin{cases} A_o(x_o, y_o) e^{\frac{i2\pi W(x_o, y_o)}{\lambda}} & x_o, y_o \in \text{aperture}, \\ 0 & x_o, y_o \notin \text{aperture}, \end{cases} \quad (2)$$

here $A_o(x_o, y_o)$ represents the amplitude distribution over the emerging wavefront at the aperture and $W(x_o, y_o)$ is the aberration function of the wavefront.

On the other hand, the amplitude field in the exit pupil image is given by the Fourier transform of Eq. (1) and is written as

$$G(x, y) = \int\int\limits_{-\infty}^{\infty} a(x_r, y_y)$$
$$\times M(x_r, y_y) e^{\frac{2\pi}{\lambda r}(x_r x + y_r x)} dx_r dy_r, \quad (3)$$

where $M(x_r, y_r)$ is the substructured grating function that acts as a filtering or modulating device.

If we assume that the stripes of the substructured grid are parallel to the *y*-axis, we can represent the substructured grating function by a complex Fourier series, given by

$$M(x_r) = \sum_{n=-\infty}^{\infty} B_n e^{\frac{i2\pi n x_r}{d}}, \quad (4)$$

where d is the ruling period and the coefficients B_n determine the transverse structure of the grating.

Then, substituting Eqs. (1) and (4) in Eq. (3), and performing the integration, the amplitude in the image plane gives

$$G(x, y) = \sum_{n-\infty}^{\infty} B_n A(x + nS, y), \quad (5)$$

where S represents the lateral shear for the first order diffracted wavefront W_n, which is given by

$$S = \frac{\lambda (r - l)}{d},\qquad(6)$$

where l represents the distance from the center of curvature of the mirror to the Ronchi grating, and n is the diffraction order for the diffracted wavefront under consideration. As discussed extensively in Ref. [7], Eq. (5) is a complicated function because repeated convolutions of the apertures lead to complex interactions between the terms of the series. But, if we consider that the intensity distribution over the exit pupil is constant, from the pupil function $A(x_o, y_o)$ given by Eq. (2), the perturbation in the image plane of the exit pupil, Eq. (5) could be written as

$$G(x, y) = \sum_{n-\infty}^{\infty} B_n e^{i\phi(x+nS,y)},\qquad(7)$$

where the phase $\phi = (x + nS, y)$ is given by

$$\phi(x + nS, y) = \frac{2\pi}{\lambda} W(x + nS, y),\qquad(8)$$

and $W(x + nS, y)$ is the laterally sheared wavefront for diffraction order n. Without loss of generality, the phase ϕ given by Eq. (8) can be conveniently decomposed as [4]

$$\phi(x + nS, y) = \phi_i + \phi_o + \phi_e,\qquad(9)$$

where ϕ_i does not depend of n, ϕ_e contains even powers of n, and ϕ_o contains odd powers of n. Substituting Eq. (9) in Eq. (7) we obtain the amplitude profile of the fringes

$$G(x, y) = e^{i\phi_i} \left\{ B_0 + 2\sum_{n=1}^{\infty} Re\left\{B_n e^{i\phi_o}\right\} e^{i\phi_e} \right\},\quad(10)$$

where we have used the fact that $\phi_e(n) = \phi_e(-n)$, $\phi_o(n) = -\phi_o(-n)$, and $B_{-n} = B_n^*$. This a general expression for the amplitude field and is valid for any wavefront.

On the other hand, if the coefficient B_n is a real number, Eq. (10) can be written as

$$G(x, y) = e^{i\phi_i} \left\{ B_0 + 2\sum_{n=1}^{\infty} B_n \cos(i\phi_o) e^{i\phi_e} \right\},\quad(11)$$

which is the same result obtained by Malacara [4] for the amplitude profile.

Finally, from Eq. (10) we obtain the intensity profile, which is given by

$$\begin{aligned} I(x, y) &= G(x, y)G^*(x, y) \\ &= \left\{ B_0 + 2\sum_{n=1}^{\infty} Re\left\{B_n e^{i\phi_o}\,\text{e}\right\} e^{i\phi_e} \right\} \\ &\times \left\{ B_0 + 2\sum_{n=1}^{\infty} Re\left\{B_n e^{i\phi_o}\right\} e^{-i\phi_e} \right\}, \end{aligned}\qquad(12)$$

this expression gives the intensity distribution in the interferometric Ronchi test and is perfectly general for any wavefront and any substructured periodic grating.
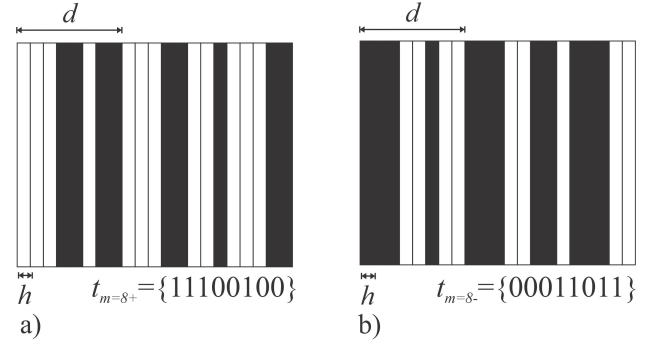

FIGURE 2. Transmittances in the substructured Ronchi gratings, a) positive 8-bit, b) negative 8-bit.

3. Substructured gratings

In this section, we design the substructure a negative and positive grating function given by Eq. (4).The substructured gratings will be Katyl-type gratings with pseudo-random Barker sequences [15]. Each substructured grating with period d, is composed of a sequence of m constituent strips of equal width h, and a transmittance t_m. Each strip is either transparent or opaque depending on the pseudo-random coding sequence used. In Fig. 2, we show the transmittances for two substructured Ronchi gratings both negative and positive. Here we consider binary sequences for lengths $m = 8$. The transmittance coefficients B_n of these substructured Ronchi gratings can be calculated using Fourier theory according to Eq. (4).

Thus, we consider an 8-bit grid with different binary sequences depending on whether the grid is positive or negative, see Fig. 2. For the positive 8-bit grid with the pseudo-random sequence $t_m = 8+ = 11100110$ [see, Fig. 2a)], we obtain that the substructured grating function can be written as

$$M^{8+}(x_r) = \frac{5h}{d} + \frac{i}{2\pi} \sum_{n=1}^{\infty} \frac{B_n^{8+} e^{\frac{i2\pi n x_r}{d}}}{n},\qquad(13)$$

where the coefficients B_n^{8+} are given by

$$B_n^{8+} = e^{\frac{-i6\pi nh}{d}} - 1 + e^{\frac{-i14\pi nh}{d}} - e^{\frac{-i10\pi nh}{d}}.\qquad(14)$$

On the other hand, for the 8-bit negative grating with transmittance $t_m = 8- = 00011001$ [Fig. 2b)] we have that the substructured grating function is given by

$$M^{8-}(x_r) = \frac{3h}{d} + \frac{i}{2\pi} \sum_{n=1}^{\infty} \frac{B_n^{8-} e^{\frac{i2\pi n x_r}{d}}}{n},\qquad(15)$$

and,

$$\begin{aligned} B_n^{8-} &= e^{\frac{-i10\pi nh}{d}} - e^{\frac{-i6\pi nh}{d}} \\ &+ e^{\frac{-i16\pi nh}{d}} - e^{\frac{-i14\pi nh}{d}}, \end{aligned}\qquad(16)$$

in both cases, the width of the strips is $h = d/8$.

4. Parabolic wavefront

For the qualitative testing of a concave parabolic mirror we will assume that $W(x + nS, y)$ is the aberration function of the wavefront by a perfect parabolic mirror which can be written as

$$W(x + nS, y) = D\left[(x + nS)^2 + y^2\right]$$
$$+ E\left[(x + nS)^2 + y^2\right]^2, \qquad (17)$$

where for simplicity in the calculations only spherical aberration E, and defocusing D terms are considered in the aberration function [4], more general wavefronts can be considered following the same idea. Setting y equal to zero, and assuming that the power in x is less or equal to 2 (here it is assumed that the fringe considered is near the center of the wavefront under test), Eq. (17) is given approximately by

$$W(x + nS, y) = 2DSxn + DS^2n^2$$
$$+ 4ES^3xn^3 + ES^4n^4. \qquad (18)$$

From Eqs. (8), (9) and (18), the phases ϕ_e and ϕ_o are given by

$$\phi_e = \frac{2\pi}{\lambda}n^2S^2\left(D + En^2S^2\right),$$
$$\phi_o = \frac{4\pi}{\lambda}nS\left(D + 2En^2S^2\right)x. \qquad (19)$$

Here the defocusing coefficient D depends on the position of the grating and is given by

$$D = \frac{l}{2r(r - l)}. \qquad (20)$$

On the other hand, for a wavefront reflected from a parabolic mirror illuminated with a point source, the spherical aberration coefficient can be written

$$E = \frac{1}{4r^3}. \qquad (21)$$

Substituting Eqs. (20) and (21) into (19), we obtain for the phase

$$\phi_e = \frac{\pi\lambda l(r - l)n^2}{rd^2}\left\{1 + \frac{n^2\lambda^2(r - l)^3}{2r^2d^2l}\right\},$$
$$\phi_o = \frac{2\pi nl}{rd}\left(1 + \frac{n^2\lambda^2(r - l)^3}{r^2d^2l}\right)x, \qquad (22)$$

these expressions are used in Eq. (12) to calculate the fringe intensity profiles for a wavefront reflected by a parabolic mirror.

Finally, to obtain sharp fringes in the interferometric Ronchi test we have considered the Talbot effect since if a Ronchi grating is illuminated with coherent waves a self-image is obtained at a characteristic distance $L = 2d^2/\lambda$ called Rayleigh distance or Talbot length [18]. For the test of a concave parabolic mirror the Talbot fringes appear when the phase ϕ_e is an integer multiple m of 2π [4]

$$l(r - l) = 2mrd^2/\lambda, \qquad (23)$$

solving for l results,

$$l = r/2 - \left\{(r/2)^2 - mrL\right\}^{1/2}, \qquad (24)$$

which is the distance from the center of curvature of the parabolic mirror to the Ronchi grating characterized by the Rayleigh distance L. In this position the images observed in the image plane, in the Ronchi configuration, are self-images of the Ronchi grating and give us sharp fringes.

5. Experimental results

To apply our theoretical results to an experimental case, we consider a parabolic mirror, which has a design radius of curvature of $r = 3000$ mm and 57.27 mm in diameter. The parabolic mirror was mounted in two linear stages to facilitate centering along the x and y directions. From the experimental point of view, we have considered the advantage of using an LCD display that allows to easily change the structure of the binary pattern of the ruling [6]. The LCD is a spatial light modulator (XGA2) that displays the substructured binary patterns with a spatial resolution of 1024×768 pixels, the dimensions of the active pixels are 23×16 mm.

The LCD was mounted in three linear stages to facilitate centering along the x, y, and z directions; this allows the defocus of the grating to be changed. The light source is an LED with a dominant wavelength of 700 nm. Images were captured with a black-and-white CCD camera (Sony Model XC-ST70), with an 8.8×6.6 mm CCD sensor, and an 8-mm focal length video lens, the experimental setup is shown in Fig. 3a). According to Section 3, we designed and constructed the substructured positive and negative gratings to perform the experiments. The period of the substructured Ronchi gratings is $d = 78$ μm. In Figs. 3b) and 3c) we show the substructured positive and negative gratings used, respectively. These substructured gratings were displayed on the LCD.

In Figs. 4-7, we show the resulting Ronchigrams with the 8-bit gratings at the Rayleigh distance in and out of focus, and at other distances and their corresponding intensity profiles. In these cases, we perform the interference with two diffraction orders, $n = 2$. For comparison, we calculated the theoretical intensity patterns for substructured positive and negative gratings by substituting Eqs. (13), (16) and (22) in Eq. (12) at different grating positions according to Eq. (24). As before, to appreciate the details of the interference patterns, for the numerical calculations we considered $n = 2$ in the diffraction order for the diffracted wavefront. Note that the experimental and calculated intensity profiles are very similar to the corresponding Ronchigrams, as expected.
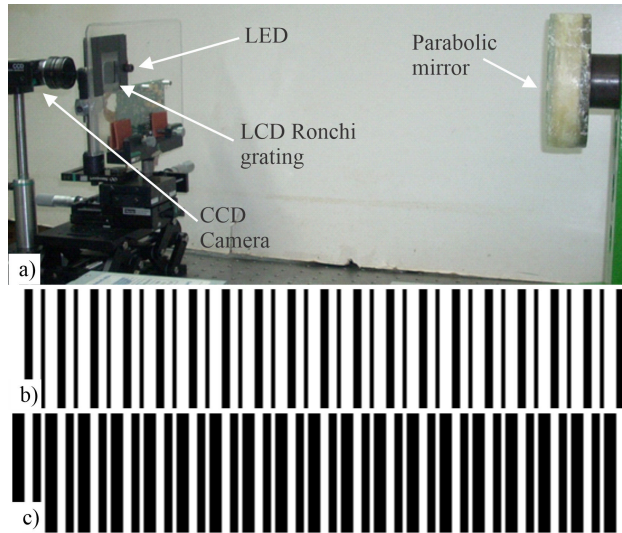
FIGURE 3. a) Experimental configuration for testing qualitatively a parabolic mirror using the Ronchi test. Substructured 8-bit Ronchi grating: b) positive, c) negative.
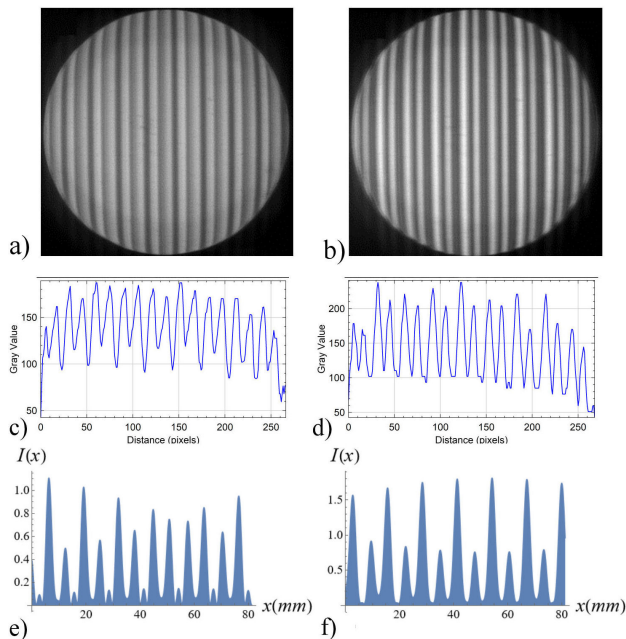

FIGURE 4. Ronchigrams images obtained with the 8-bit gratings: a) positive, b) negative. Experimental intensity profile: c) positive, d) negative. Theoretical intensity profile: e) positive, f) negative. In-focus at the Rayleigh distance at $l = 17.28$ mm.

In Figs. 4a) and 4b) we see the Ronchigrams images obtained for the 8-bit positive and negative gratings, respectively. These Ronchigrams were taken when the Ronchi gratings are placed in-focus at the Rayleigh distance $l = 17.28$ mm measured from the center of curvature of the parabolic mirror, this distance is calculated with Eq. (24).

To give an approximate quantitative value for fringe contrast, we must consider that contrast is nothing more than a measure of the difference between the maximum and minimum gray level of a fringe measured in pixels [19,20]. Thus,

if the contrast is given by $C = (P_{max} - P_{min})/(P_{max} + P_{min})P_{max}$ with P_{max} being the maximum gray value and P_{min} the minimum gray value for a fringe, then for a fringe in Figs. 4a) and 4b), the contrast is $C = 53.23$ and $C = 98.82$, respectively. Therefore, the negative grating provides better fringe contrast than the positive grating. Figures 4c) and 4d) show the experimental intensity profiles obtained from Figs. 4a) and 4b), respectively with $y = 0$. From these plots is easy to see that the negative grating gives better fringe contrast than the positive grating. Conversely, Figs. 4e) and 4f) show the corresponding theoretical fringe intensity profile for the 8-bit for the positive and negative grating calculated from Eq. (21), respectively. A detailed qualitative analysis of these plots shows how the calculated intensity patterns correspond with those obtained experimentally, for both substructured gratings, Figs. 4a) and 4b).

On the other hand, by placing the Ronchi substructured grating out of focus at the Rayleigh distance at $l = -17.48$ mm from the center of curvature of the mirror, we obtain the Ronchigrams show in Figs. 5a) and 5b) for the positive and negative 8-bit gratings, respectively. Figs. 5c) and 5d) show the experimental intensity profiles obtained from Figs. 5a) and 5b), respectively with $y = 0$. Figs. 5e) and 5f) show the corresponding theoretical fringe intensity profile for the 8-bit gratings: 5e) Positive, and 5f) negative calculated with Eq. (4). As before, for a fringe in Figs. 5a) and 5b), the contrast is $C = 51.17$ and $C = 95.23$, respectively. Therefore, the fringes of the negative grating are sharper than those of the positive grating.

In addition, in Figs. 6a) and 6b) we show the corresponding Ronchigrams of the substructured grating at an arbitrary
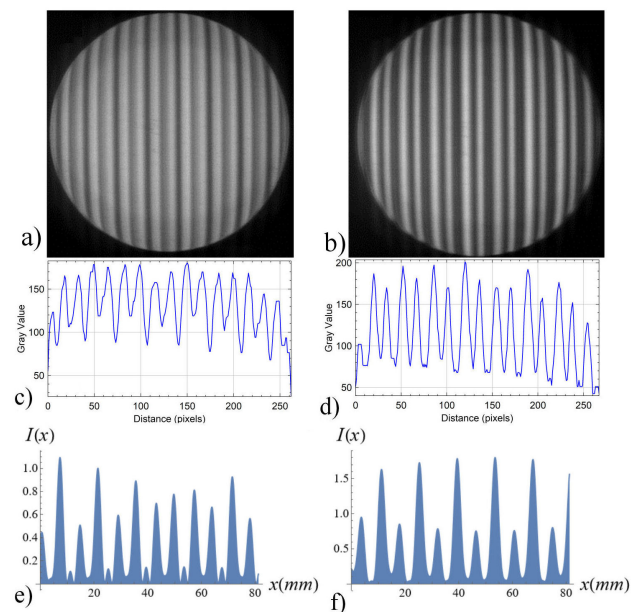

FIGURE 5. Ronchigrams images obtained with the 8-bit gratings: a) positive, b) negative. Experimental intensity profile: c) positive, d) negative. Theoretical intensity profile: e) positive, f) negative. Out of focus at the Rayleigh distance at $l = -17.48$ mm.
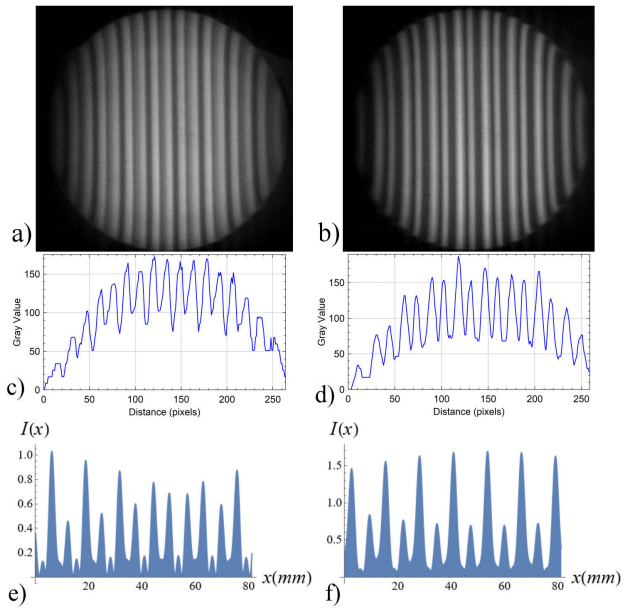
FIGURE 6. Ronchigrams images obtained with the 8-bit gratings: a) positive, (b) negative. Experimental intensity profile: c) positive, d) negative. Theoretical intensity profile: e) positive, f) negative. Out of focus at $l = -17.28$ mm.
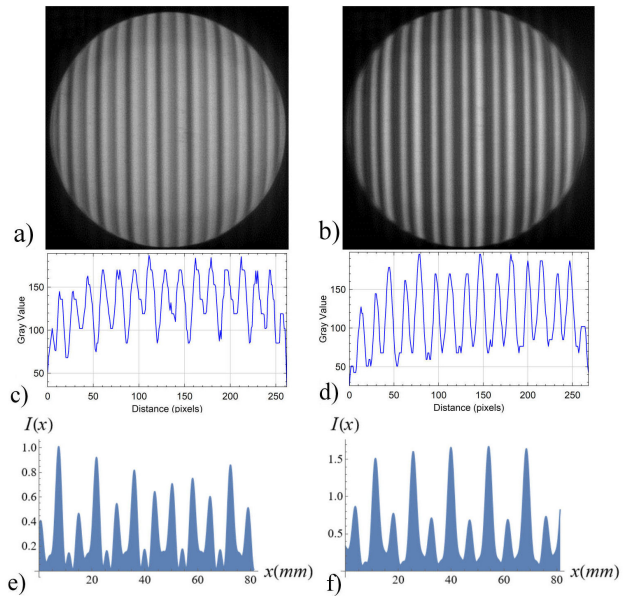

FIGURE 7. Ronchigrams images obtained with the 8-bit gratings: a) positive, b) negative. Experimental intensity profile: c) positive, d) negative. Theoretical intensity profile: e) positive, f) negative. In-focus at $l = 17.48$ mm.

out of focus distance at $l = -17.28$ mm for the 8-bit positive and negative grating, respectively. In this case, the contrast in Fig. 6a) is 56.06 and the contrast in Fig. 6b) is 72.97. From these contrast values and the experimental plots [Figs. 6c) and 6d)] and the theoretical plots [Figs. 6e) and 6f)] we conclude that the fringes are not sharp enough for this distance. Similarly, Fig. 7 shows the Ronchigrams results obtained for in-focus positive and negative substructured grating placed at
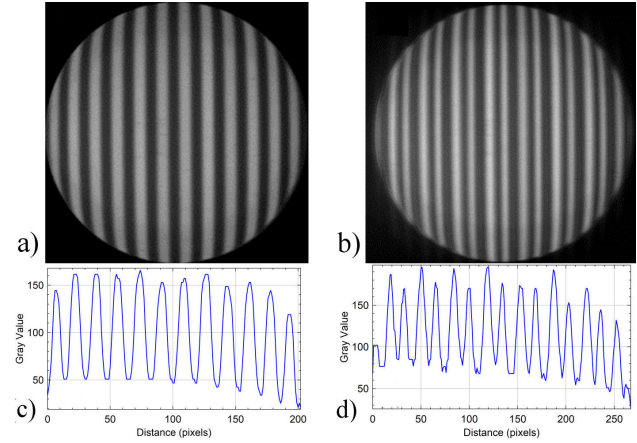

FIGURE 8. Ronchigrams images obtained with: a) classical grating, b) substructured 8-bit negative grating. Fringe intensity profile for: c) classical grating, d) substructured 8-bit negative grating.

a distance $l = 17.48$ mm. Here, the contrast in Fig. 7a) is 62.76 and that of Fig. 7b) is 92.42. In these instances, we can see that the fringes for these substructured grid positions are not as sharp.

Finally, to show that the use of substructured gratings in the Ronchi test provides better contrast and that the strips reflected by the test surface are sharper, in Figs. 8a) and 8b), we show Ronchigrams corresponding to a classical grating and a substructured grating, respectively. The classical grating was placed at the paraxial focus, and the substructured grating was placed inside the focus at the Rayleigh distance. The image of the substructured grating corresponds to an 8-bit negative grating Figs. 8c) and 8d) show the intensity profiles corresponding to the classical grating and the 8-bit substructured grating, respectively. In this case, the fringe contrast is 78.83 for Fig. 8a) and 92.03 for Fig. 8b), indicating that the fringes corresponding to the 8-bit substructured grating are sharper than those of the classical grating.

6. Conclusions

In this work, we proposed to use substructured gratings to increase the sharpness of the fringes. Each grating period is divided into several stripes of equal width that can be transparent or opaque; the transmission coefficients of the stripes along the grating period are not periodic, but a previously chosen binary sequence.

The experimental results are presented for qualitative testing of a parabolic mirror of 3000 mm radius of curvature and 57.27 mm diameter. Experimentally we find that the fringes are sharper at the Rayleigh distance inside and outside the mirror focus for the negative substructured grating. These results agree with the numerically obtained profiles. We find that if the Ronchi grating is placed inside focus at Rayleigh distance in $l = -17.48$ mm and outside the focus at distance $l = 17.28$ mm, we have a high fringe contrast. On the other hand, fringe contrast is low with defocus magnitudes of

Ronchi grating axial position equal to $l = 17.48$ mm and $l = -17.28$ mm.

The results show that, in order to obtain sharper stripes in the Ronchi test, the structure of the Ronchi grating and its position play a crucial role. Furthermore, these results provide specific positions for the grating that must be reached during the experiments; otherwise, the fringes will be as coarse as with classical Ronchi gratings. This approach is simple to apply and can facilitate work in the optics shop during the fabrication process of an optical surface.

Acknowledgments

1. V. Ronchi, Forty Years of History of a Grating Interferometer, *Appl. Opt.* **3** (1964) 437, https://doi.org/10.1364/AO.3.000437.

2. A. Cornejo-Rodríguez, Ronchi test, Optical Shop Testing **3** (2007).

3. R. Juarez-Salazar, Nonparaxial geometrical Ronchi test for spherical mirrors: an inverse ray-tracing approach, *Appl. Opt.* **55** (2016) 5986, https://doi.org/10.1364/AO.55.005986.

4. D. Malacara, Analysis of the interferometric Ronchi test, *Appl. Opt.* **29** (1990) 3633, https://doi.org/10.1364/AO.29.003633.

5. D. Aguirre-Aguirre *et al.*, Simulation algorithm for ronchigrams of spherical and aspherical surfaces, with the lateral shear interferometry formalism, *Optical Review* **20** (2013) 271, https://doi.org/10.1007/s10043-013-0049-7.

6. J. Castro-Ramos, S. Vazquez-Montiel, and A. Padilla-Vivanco, Phase shifting interferometry by using an LCD and bironchi test, In A. M. O. and J. L. Paz, eds., 5th Iberoamerican Meeting on Optics and 8th Latin American Meeting on Optics, Lasers, and Their Applications, vol. 5622, International Society for Optics and Photonics (SPIE, 2004) pp. 639 - 645, https://doi.org/10.1117/12.591802.

7. E. Luna *et al.*, High-resolution phase-shifting Ronchi test, *Appl. Opt.* **61** (2022) 7875, https://doi.org/10.1364/AO.468068.

8. D. Aguirre-Aguirre *et al.*, Algorithm for Ronchigram recovery with random aberrations coefficients, *Optical Engineering* **52** (2013) 053606, https://doi.org/10.1117/1.OE.52.5.053606.

9. R. Barakat, General Diffraction Theory of Optical Aberration Tests, from the Point of View of Spatial Filtering, *J. Opt. Soc. Am.* **59** (1969) 1432, https://doi.org/10.1364/JOSA.59.001432.

10. F. Cooke, M. V. R. K. Murty, and A. Cornejo, Sharpening the Fringes in the Ronchi Test, *Appl. Opt.* **12** (1973) 2230, https://doi.org/10.1364/AO.12.002230.

11. J. Salinas-Luna *et al.*, Ronchi test with variable-frequency rulings, *Optical Engineering* **48** (2009) 013604, https://doi.org/10.1117/1.3072956.

12. M. M. González and N. A. Ochoa, The Ronchi test with an LCD grating, *Optics Communications* **191** (2001) 203, https://doi.org/10.1016/S0030-4018(01)01141-5.

13. M. Mora-Gonzalez and N. A. Ochoa, Sinusoidal liquid crystal display grating in the Ronchi test, *Optical Engineering* **42** (2003) 1725 , https://doi.org/10..1117/1.1572890.

14. D. Aguirre-Aguirre, et al., Substructured Ronchi gratings from the linear combination of classical gratings, *Optical Engineering* **53** (2014) 114111, https://doi.org/10.1117/1.OE.53.11.114111.

15. R. H. Katyl, Moiré Screens Coded with Pseudo-Random Sequences, *Appl. Opt.* **11** (1972) 2278, https://doi.org/10.1364/AO.11.002278.

16. M. Campos-Garcia and F.-S. Granados-Agustin, Interferometric Ronchi test by using substructured gratings, In H. Bosse, B. Bodermann, and R. M. Silver, eds., Modeling Aspects in Optical Metrology II, vol. 7390, International Society for Optics and Photonics (SPIE, 2009) p. 73901B, https://doi.org/10.1117/12.827302.

17. D. Aguirre-Aguirre *et al.*, Evaluation of the increment of the sampling in optical testing using substructured Ronchi gratings, *Journal of Physics: Conference Series* **274** (2011) 012062, https://doi.org/10.1088/1742-6596/274/1/012062.

18. J. Wen, Y. Zhang, and M. Xiao, The Talbot effect: recent advances in classical optics, nonlinear optics, and quantum optics, *Adv. Opt. Photon.* **5** (2013) 83, https://doi.org/10.1364/AOP.5.000083.

19. E. Peli, Contrast in complex images, *J. Opt. Soc. Am. A* **7** (1990) 2032, https://doi.org/10.1364/JOSAA.7.002032.

20. P. J. Bex and W. Makous, Spatial frequency, phase, and the contrast of natural images, *J. Opt. Soc. Am. A* **19** (2002) 1096, https://doi.org/10.1364/JOSAA.19.001096.